RSC Advances

PAPER

View Article Online
View Journal | View Issue

Cite this: RSC Adv., 2014, 4, 44509

Steric and electronic control over the structural diversity of *N*-(*n*-pyridinyl) diphenylphosphinic amides ($n = 2$ and 4) as difunctional ligands in triphenyltin(IV) adducts†

K. Gholivand,*[a] A. Gholami,[a] S. K. Tizhoush,[a] K. J. Schenk,[b] F. Fadaei[b] and A. Bahrami[a]

Received 25th June 2014
Accepted 9th September 2014

DOI: 10.1039/c4ra06212d

www.rsc.org/advances

Two triphenyltin(IV) adducts of difunctional ligands, *N*-(*n*-pyridinyl) diphenylphosphinic amide ($n = 2$ and 4), have been synthesized and characterized by ^{1}H, ^{31}P, ^{119}Sn NMR and IR spectroscopy. The spectroscopic properties of the complexes were compared with those of corresponding ligands. The crystal structures of the complexes were determined by X-ray crystallography, which reveals a trigonal bipyramidal geometry surrounding the tin(IV). Both of the ligands function in an ambidentate mode, ligating through either the O or N atom. The experimental and theoretical (DFT) studies show that the Sn(IV) interacts more strongly with the *N*-pyridine atom than the P=O functional group. Furthermore, DFT calculations, at the B3LYP level, have been carried out to determine the deeper reasons for the adopted bonding mode in the complexes. The influence of the ligand structure on the coordination behaviour and the contribution of hydrogen bonding to the stability of the resulting complexes were elucidated. The results indicate that the intermolecular hydrogen bonds have an important role in the molecular structures and supramolecular associations of the organotin(IV) compounds.

Introduction

The development of well-designed ligand systems with which the properties of their complexes can be easily varied in a controlled manner is one of the most important goals in modern inorganic and organometallic chemistry. Among the many ligand systems in the literature, heterodifunctional ligands[1–8] are intensively studied and applied owing to the often unique properties of their metal complexes. The coordination chemistry of such ligands, capable to realize different binding modes with metal centers,[9] is interesting for synthesis of new selective complexing agents and analytical reagents.

In this regard, our group has made considerable effort to study the ligation behavior of phosphoramidate ligands containing additional donor sites such as carbonyl or/and *N*-pyridine particularly toward organotin(IV) compounds.[10–15] Much of the interest in organotin(IV) complexes arises from their catalytic and biological activity.[16–21] Studies on organotin(IV) derivatives containing mixed N,O-ligands have revealed considerable structural diversity which may lead to complexes with different properties.[22–24] However, the basis of their selectivity remains poorly understood.

In the present work, we consider phosphoramidate ligands based on aminopyridine with different distance between the donor sites of phosphoryl and *N*-pyridine. The main reasons for the selection of these ligands are the different nature of the two coordinating sites as well as various positions of them relative to each other that creates variety of potential coordination modes. From the structural chemistry aspect it is interesting to give reasons for the type of adopted bonding mode. We approach the problem by a combined theoretical-practical point of view.

Accordingly, we have carried out a comparative study on the triphenyltin(IV) adducts of *N*-(*n*-pyridinyl) diphenylphosphinic amides (where $n = 2$ and 4 in ligand $\mathbf{L_1}$ and $\mathbf{L_2}$, respectively). Crystal structures of the complexes $\mathbf{C_1}$ and $\mathbf{C_2}$ were determined by X-ray crystallography, which revealed the different coordination behaviour of the two ligands. The bonding, electronic and energy aspects of all compounds were considered using quantum mechanical calculations. Furthermore, the influence of the ligand structure on the stereoselectivity of bond formation and the contribution of hydrogen bonds in the structure and directing the crystal packing of complexes were elucidated.

[a]Department of Chemistry, Faculty of Basic Sciences, Tarbiat Modares University, P.O. Box 14115-175, Tehran, Iran. E-mail: gholi_kh@modares.ac.ir; Fax: +98-021-88009730; Tel: +98-21-82884422

[b]École Polytechnique Fédérale de Lausanne, CCC-IPSB, Le Cubotron Dorigny, 1015 Lausanne, Switzerland

† Electronic supplementary information (ESI) available: The crystal data and the details of the X-ray analysis, selected bond lengths and bond angles. CCDC 978396 ($\mathbf{C_1}$), 978395 ($\mathbf{C_2}$). For ESI and crystallographic data in CIF or other electronic format see DOI: 10.1039/c4ra06212d

Results and discussion

Synthesis and spectroscopic characterization

Various molar ratios of ligand: $SnPh_3Cl$ were assessed in the crystallization, since we were not certain which coordination modes would prevail. But evaporation from 1 : 1 solutions of $HCCl_3$: heptane, at room temperature, yielded only two crystals suitable for X-ray diffraction. For the ligand $\mathbf{L_1}$, the five-coordinated complex $\mathbf{C_1}$ grew from a 1 : 1 ratio, and for the ligand $\mathbf{L_2}$, the ratio 1 : 2 afforded the five-coordinated mononuclear complex $\mathbf{C_2}$. Therefore, we may conjecture that the formation of $\mathbf{C_2}$ is independent of the molar ratio, but is rather driven by the steric and electronic features of the ligand $\mathbf{L_2}$. Selected spectroscopic data of organotin compounds and their corresponding ligands are listed in Table 1.

The coordination mode of the ligands can be reliably followed by the IR spectroscopy. The considerable negative shift of the $\upsilon_{(P=O)}$ in the spectra of $\mathbf{C_1}$ by 24 cm^{-1} with respect to the free ligand, demonstrates the coordination of the phosphoryl group to tin like in many other complexes of phosphoramidates.[10–15,25,26] The $\upsilon_{(py\ ring)}$ of the complex $\mathbf{C_1}$ (1591 cm^{-1}) do not differ from the frequencies for the free ligand. Interestingly, an opposite shift was observed for the P=O frequency of $\mathbf{C_2}$ with respect to the free ligand $\mathbf{L_2}$. The main change in the spectra of $\mathbf{C_2}$ deal with the increasing of $\upsilon_{(py\ ring)}$ band by 19 cm^{-1} while the $\upsilon_{(P=O)}$ value is close to that of the free ligand. This observation can be explained by the coordinating from N_{py} site to Sn in this complex. The same results are also, evident from the X-ray crystallographic structures for $\mathbf{C_1}$ and $\mathbf{C_2}$ (Fig. 1 and 3).

The absorption band at 3117 cm^{-1} in $\mathbf{L_1}$ is attributed to the N–H stretching mode which shifts toward higher frequency in $\mathbf{C_1}$. This positive shift may be due to the weakening of the hydrogen bonds from $N–H\cdots O_{P=O}$ in $\mathbf{L_1}$, which is a common hydrogen bonding in the phosphoramide ligands,[10–15] to $N–H\cdots N_{py}$ in the coordinated species $\mathbf{C_1}$. Although the N–H groups of $\mathbf{L_2}$ and $\mathbf{C_2}$ are involved in the same intermolecular interactions, $N–H\cdots O_{P=O}$, the position of this bond in these compounds also indicates the weaker hydrogen bonding in the structure of $\mathbf{C_2}$ relative to the ligand $\mathbf{L_2}$.

The ^{1}HNMR spectral data obtained for the ligands suggest the expected structure of these molecules. However, the chemical shifts and the ^{1}H-coupling constants of ligands are almost insensitive to complexation. Furthermore, chemical shift of ^{31}P for the ligands are quite similar to those of the corresponding complexes. These data don't provide any concrete information about the tin-ligand coordination. The single resonance in the ^{119}SnNMR spectrum of $\mathbf{C_1}$ at −50 ppm is in agreement with the reported value for free $SnPh_3Cl$ (−44.7),[27] indicating that the triphenyltin chloride complex $\mathbf{C_1}$ is kinetically labile on the ^{119}SnNMR time scale. This is consistent with other triphenyltin(IV) adducts which are not stable in solution.[28] Although, the ^{119}Sn resonance for $\mathbf{C_2}$ shifts to −74 ppm, such chemical shift is not still in the range for the five-coordinated tin compounds (from −90 to −190 ppm).[29] This might be a hint to an equilibrium between the adduct $Ph_3SnCl\cdot$ligand and Ph_3SnCl + ligand that, at ambient temperature, is fast on the NMR time scale.[28]

Besides, the ^{119}Sn chemical shift, in comparison with the shift of pure Ph_3SnCl, points to the relative population of free Ph_3SnCl and its complex in the equilibrium. Comparing the ^{119}SnNMR spectrum of two complexes reveals that the Sn–L interaction is stronger for $\mathbf{C_2}$ (through the N_{py} donor) in solution, in accordance with the result from solid-state structures and gas phase computations.

Table 1 Spectroscopic data of compounds

Compound	$\upsilon_{(N-H)}$ (cm^{-1})	$\upsilon_{(P=O)}$ (cm^{-1})	$\upsilon_{(py\ ring)}$ (cm^{-1})	$\delta(^{31}P)$ (ppm)	$\delta(^{119}Sn)$ (ppm)
Ligand					
$\mathbf{L_1}$	3117	1185	1591	18.8	—
$\mathbf{L_2}$	3203	1182	1595	19.5	—
Complex					
$\mathbf{C_1}$	3442	1161	1591	18.8	−50
$\mathbf{C_2}$	3440	1187	1614	19.6	−74

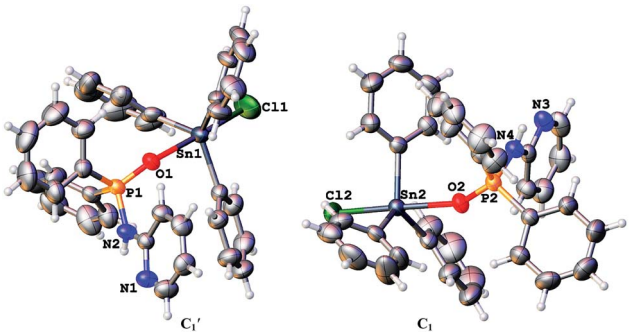

Fig. 1 The molecular structure of $\mathbf{C_1}$ with its atom (50% probability level) labelling scheme. Hydrogen atoms were omitted for clarity.

X-ray crystallography investigation

Colorless single crystals of both complexes were obtained from solutions of chloroform–heptane by slow evaporation at room temperature. Crystal data and details of the X-ray analysis are given in Table S1.† Selected bond lengths and angles are summarized in Tables S2 and S3† and hydrogen bonds in Table 2. Molecular structures and packing diagrams are shown in Fig. 1–4.

Crystal structure of *N*-(2-pyridinyl)diphenylephosphinic amide-κ-*O* chlorotriphenyltin(IV) ($\mathbf{C_1}$)

The title complex crystallizes in the space group $C2/n$ with $Z' = 2$. In each conformer ($\mathbf{C_1}$ and $\mathbf{C_1'}$, Fig. 1), the ligand binds in a unidentate manner through the phosphoryl donor. The coordination polyhedra of tin can be described as distorted trigonal bipyramid (three phenyls equatorial, chlorine and the phosphoryl at the apices). The *trans* angles around tin are Cl1–Sn1–O1 = 178.21(5)° and Cl2–Sn2–O2 = 176.99(4)°, and the sum of angles in the trigonal girdle around Snare 358.66° ($\mathbf{C_1}$) and 358.16° ($\mathbf{C_1'}$). Bonding parameters agree with values found for similar geometries.[10,30,31] As expected, the shorter Sn–O distance

Table 2 Hydrogen-bonding data[a] for the X-ray structures

Compound	D–H–A	d(D–H)	d(H···A)	d(D···A)	<DHA
$\mathbf{C_1}$	N(2)–H(200)···N(3)$^{b(i)}$	0.78 [1.022]	2.57 [2.329]	3.324(3)	163 [163.20]
	N(4)–H(400)···N(1)$^{b(ii)}$	0.74 [1.027]	2.29 [2.006]	3.004(3)	162 [163.94]
$\mathbf{C_2}$	N(2)–H(22)···O(2)$^{b(iii)}$	0.86 [1.025]	2.04 [1.824]	2.835(4)	153 [168.21]
	N(4)–H(44)···O(1)$^{b(iv)}$	0.86 [1.019]	2.19 [1.848]	2.802(4)	128 [154.27]

[a] The values in the brackets refer to the calculated parameters at the B3LYP/LANL2DZ/6-311G* level. [b] Symmetry codes: (i) $[x, -1+y, -1+z]$; (ii) $[x, 1+y, 1+z]$; (iii) $[-1+x, y, -1+z]$; (iv) $[x, y, 1+z]$.

(in $\mathbf{C_1}$: 2.4031(14) Å) corresponds to the larger P–O–Sn angle (in $\mathbf{C_1}$: 154.60(9)°). Beside, the Sn–O bond shortening is also accompanied by an increase in the Sn–Cl bond length (2.4820(6) Å in $\mathbf{C_1}$) because of the greater *trans* influence.

$\mathbf{C_1}$ and $\mathbf{C_1'}$ are joined to dimers by means of weak N–H···N_{py} hydrogen bonds between the amidic groups and the pyridine rings (Table 2). Other weak interactions susceptible to stabilize the structure include: (i) intermolecular hydrogen bonding including C–H···Cl (with C···Cl distances 3.681(11) and 3.767(4) Å) and (ii) C–H···π interactions (C5–H5···Cg: $d_{H\cdots Cg}$ = 3.08 Å, $d_{C\cdots Cg}$ = 3.927(3) Å, θ = 152° and C76A–H76A··· Cg: $d_{H\cdots Cg}$ = 2.84 Å, $d_{C\cdots Cg}$ = 3.72(2) Å, θ = 159°: Cg is the centroid of py rings and θ is the angle of C–H···Cg). These intermolecular interactions generate a 3D structure in the crystal (Fig. 2).

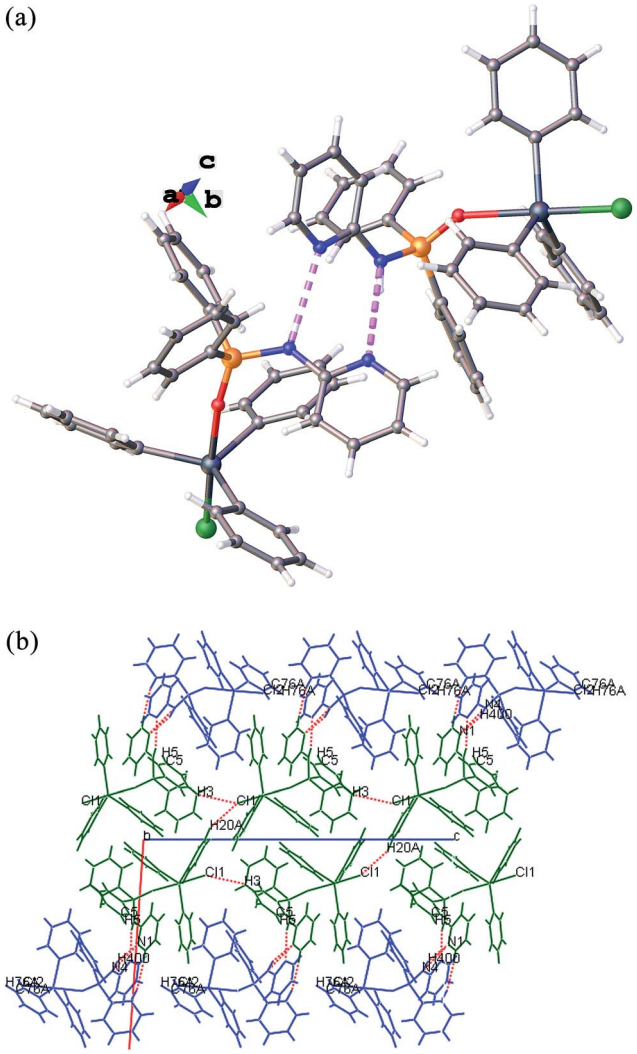

Fig. 2 (a) Dimeric tin aggregate, showing intermolecular hydrogen bonds between two conformers and (b) packing diagram of $\mathbf{C_1}$ formed by supramolecular interactions.

Crystal structure of *N*-(4-pyridinyl)diphenylephosphinic amide-κ-*N* chlorotriphenyltin(IV). *N*-(4-pyridinyl) diphenylphosphinic amide ($\mathbf{C_2}$)

The compound $\mathbf{C_2}$ crystallizes in the space group $P\bar{1}$. Its structure consists of an uncoordinated ligand and a tin adduct held together by hydrogen bonds. The ligand $\mathbf{L_2}$ coordinates in a monodentate mode, from the nitrogen site of the pyridine ring toward the tin atom. The central tin atom (Fig. 3) lies in a distorted trigonal bipyramide formed by three phenyl groups (Sn–C(16), 2.125(3); Sn–C(22), 2.135(3) and Sn–C(28) 2.125(3) Å) in the equatorial plane, one chloride ion (Sn–Cl, 2.5029(9) Å) and the *N*-pyridine atom (Sn–N_{py}, 2.553(3) Å) in the apical (*trans*) positions. The sum of the angles subtended at tin in the trigonal girdle is 358.8°, and the *trans* angle presents little deviation from linearity (Cl–Sn–N_{py} 175.82(7)°). The Sn–C and Sn–Cl bond lengths are in the range of the covalent band[32,33] while the Sn–N bond is in accordance with the coordinate bond.[34] It is worthy to note that similar bonding parameters of the coordinated and free ligand present in the crystal $\mathbf{C_2}$ do not differ significantly.

In the structure of $\mathbf{C_2}$, moderately strong N-H_{amidic}···$O_{P=O}$ hydrogen bonds (Table 2) build up alternating [100] chains of tin adducts and free ligands; which are further reinforced by weaker C–H···Cl hydrogen bonds between a phenyl group, H53, of the ligand and the chlorine atom on the tin complex. The same kind of H-bond is also the driving force in generating a 3D

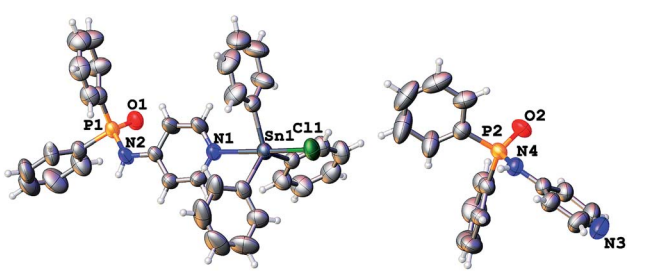

Fig. 3 The molecular structure of $\mathbf{C_2}$ with its atom (50% probability level) labelling scheme. Hydrogen atoms were omitted for clarity.

network (Fig. 4); indeed, tin adducts of neighbouring chains are linked *via* C–H···Cl interactions between hydrogen atoms of phenyl rings connected to the chlorine atom of tin adduct (H3 creates a [010] chain, and H9 a [001] one). The donor–acceptor distances of 3.664(5) and 3.717(4) Å are in the expected region reported for this type of hydrogen bonds.[23,35] It is finally worth noting that the pair of neighbouring free ligands is distinguished by a doublet of parallel CH···π interactions (C65–H65···Cg: $d_{H\cdots Cg} = 3.33$ Å, $d_{C\cdots Cg} = 3.914(5)$ Å, $\theta = 123.07°$: Cg is the centroid of py ring).

Comparison of the structures for complexes C_1 and C_2

Both of *N*-(pyridinyl)diphenylephosphinic amides $\mathbf{L_1}$ and $\mathbf{L_2}$ function as ambidentate ligands, ligating through either the O or N atom. The ligand $\mathbf{L_1}$ coordinates *via* phosphoryl group in the structure $\mathbf{C_1}$, while the other one acts as an N-donor in the crystal $\mathbf{C_2}$. There is a chlorine atom in the *trans* position of each coordinating atom and Sn–Cl distances are in the reverse correlation with the binding strength of the donors. The lengthening of Sn–Cl bond in $\mathbf{C_2}$ indicates a higher donating ability of N_{py} with respect to O_p (*trans* influence).

Since the Sn–N bond is stronger than the Sn–O one, it was expected that the nitrogen atom coordinated to tin rather than the phosphryl oxygen. However, it seems that coordination of N_{py} is inhibited in $\mathbf{C_1}$, owing to a steric factor. The ambidentate manner of $\mathbf{L_1}$ instead of the chelating arrangement in question may be also caused by steric hindrances due to the presence of three bulky phenyl groups on tin. The steric control over the molecular structure of organotin compounds have been noticed previously.[22,30] The most striking feature of the compound $\mathbf{C_2}$ is behaviour of the ligand which is unusual in not coordinating to tin, alternately. Adjacent coordinated and uncoordinated ligands are linked *via* effective intermolecular $N–H_{amidic}\cdots O_{P=O}$ interactions.

As a result of different binding modes in complexes, molecular associations are different in their crystal lattices. 2-Fold linkages of neighboring conformers $\mathbf{C_1}$ and $\mathbf{C_1'}$ *via* intermolecular contacts, giving rise to the formation of dimeric tin aggregates, while one-dimensional chains in $\mathbf{C_2}$ are in consequence of hydrogen bonds between the phosphoryl and amidic groups which are anti with respect to each other (Fig. 2a and 4a).

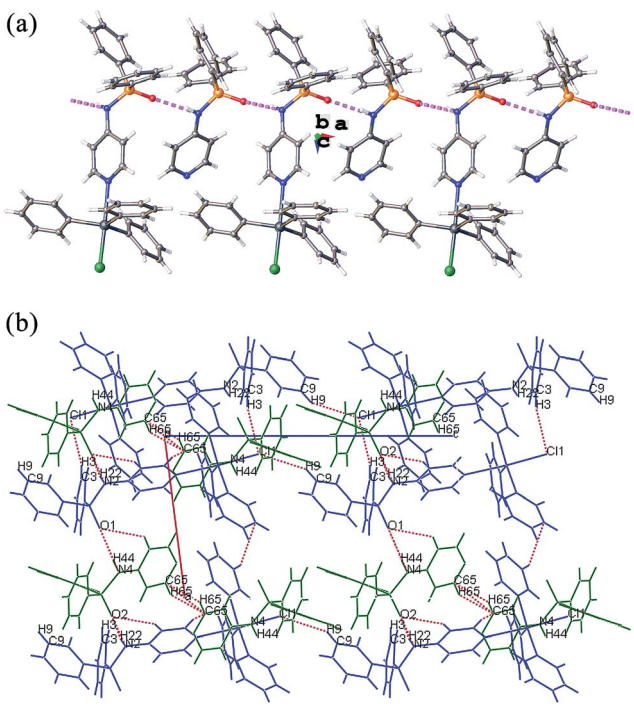

Fig. 4 (a) 1D polymeric chain along *a*-axis, showing intermolecular hydrogen bonds and (b) packing diagram of $\mathbf{C_2}$ formed by supramolecular interactions.

Computational study

The optimized structures of ligands and resulting complexes are represented in Fig. S1† and some selected bond lengths for fully optimized geometries given in Table 3. It should be mentioned that the corresponding distances in hydrogen-bonded clusters are equal to the experimental values, due to the freezing of non-hydrogen atoms in the calculations. In order to evaluate the electronic and energy aspects of compounds, the NBO calculations were performed and the results are shown in Table 4. Moreover, electron delocalization energies, E^2, from the NBO analysis and binding energies, ΔE, of some notable interactions including coordination and hydrogen bonds (Table 5) are calculated to characterize the strength of these donor–acceptor interactions. The former refers to stabilization energy of electron delocalization between the donor–acceptor orbitals, while the binding energy is related to the sum of total attractive and repulsive forces between two bonded fragments.

Electronic parameters of compounds

As seen in Tables 3 and 4, from structural and electronic points of view, the fully optimized ligands $\mathbf{L_1}$ and $\mathbf{L_2}$ are very close to each other and in a good agreement with free ligand in the cluster $\mathbf{C_2}$ ($\mathbf{L_2'}$). However, in the *ortho*-pyridinyl phosphoramidate $\mathbf{L_1}$, the negative charge localized on N_{Py} atom, $q(N_{Py})$, is larger in magnitude and also the hybridization of the lone pair of this atom, $LP(N_{Py})$, takes a more p character. The charge transfer from non-bonding orbital of the N_{amidic} atom to anti-bonding orbital C–N_{py} in the ligand $\mathbf{L_1}$ is responsible for the different electronic features of $\mathbf{L_1}$ and $\mathbf{L_2}$. The NBO analysis shows the stabilizing energy E^2 of 37.04 kcal mol^{-1} for the electronic delocalization $LP(N_{amidic}) \rightarrow \sigma^*(C–N_{py})$. Beside, the

Table 3 Striking calculated bond lengths (d, Å) at B3LYP/6-311G*-LANL2DZ level for the optimized geometries

Compound	$\mathbf{L_1}$	$\mathbf{L_2}$ ($\mathbf{L_2'}$)	Binuclear model
d(P=O)	1.495	1.494 (1.484)	1.503
d(P–N_{amide})	1.701	1.710 (1.657)	1.706
d(H–N_{amide})	1.011	1.010 (1.019)	1.010
d(Sn–$O_{P=O}$)	—	—	2.496
d(Sn–N_{py})	—	—	2.674
d(Sn–$Cl_{trans\ to\ O}$)	—	—	2.459
d(Sn–$Cl_{trans\ to\ N}$)	—	—	2.466

Table 4 Atomic charges, natural electron configurations, hybridizations at B3LYP/6-311+G*-LANL2DZ level (from the NBO analysis)

	Atomic Charge			NEC		Hybridization	
Compound	$q(O_{P=O})$	$q(N_{py})$	q(Sn)	$O_{P=O}$	N_{py}	$LP(O_{P=O})$	$LP(N_{py})$
Free Ligands							
$\mathbf{L_1}$	−1.067	−0.502	—	[Core] $2s^{1.80}$ $2p^{5.25}$	[Core] $2s^{1.36}$ $2p^{4.12}$ $3d^{0.01}$ $4p^{0.01}$	$sp^{0.51}$	$sp^{2.54}$
$\mathbf{L_2}$	−1.062	−0.478	—	[Core] $2s^{1.80}$ $2p^{5.25}$	[Core] $2s^{1.38}$ $2p^{4.08}$ $3p^{0.01}$ $3d^{0.01}$ $4p^{0.01}$	$sp^{0.52}$	$sp^{2.39}$
$\mathbf{L_2}'$	−1.096	−0.460	—	[Core] $2s^{1.80}$ $2p^{5.26}$	[Core] $2s^{1.36}$ $2p^{4.33}$ $3p^{0.01}$ $d^{0.01}$	$sp^{0.56}$	$sp^{2.34}$
Real complexes							
$\mathbf{C_1}$[a]	−1.134	−0.526	2.091	[Core] $2s^{1.76}$ $2p^{5.36}$ $3p^{0.01}$	[Core] $2s^{1.36}$ $2p^{4.15}$ $3p^{0.01}$ $3d^{0.01}$ $4p^{0.01}$	$sp^{0.74}$	$sp^{2.53}$
$\mathbf{C_2}$	−1.122	−0.547	2.119	[Core] $2s^{1.79}$ $2p^{5.33}$	[Core] $2s^{1.35}$ $2p^{4.16}$ $3s^{0.01}$ $3p^{0.01}$ $4p^{0.01}$	$sp^{0.60}$	$sp^{2.55}$
Model complex							
Binuclear	−1.114	−0.542	2.160	[Core] $2s^{1.77}$ $2p^{5.33}$ $3p^{0.01}$	[Core] $2s^{1.36}$ $2p^{4.16}$ $3p^{0.01}$ $4p^{0.01}$	$sp^{0.58}$	$sp^{2.58}$

[a] The mean values are represented for two conformers.

Table 5 D–A distances, E^2 (Electron delocalization energies (kcal mol^{-1})) and ΔE (binding energies (kcal mol^{-1}))

	$Sn–O_{P=O}$			$Sn–N_{py}$			$P=O\cdots HN_{amide}$			$N_{py}\cdots HN_{amide}$		
Compound	d	E^{2a}	ΔE	d	E^{2a}	ΔE	d	E^{2b}	ΔE	d	E^{2b}	ΔE
$\mathbf{C_1}$	2.403	26.28	12.14	—	—	—	—	—	—	3.323	5.02	4.88
	2.463	22.20	11.78							3.004	13.66	
$\mathbf{C_2}$	—	—	—	2.553	34.64	12.43	2.801	10.80	8.23	—	—	—
							2.836	10.24	5.05			
Binuclear model	2.496	25.89	8.78	2.674	27.76	8.82	—	—	—	—	—	—

[a] LP(1) donor to LP* Sn. [b] LP(1) donor to σ* HN_{amid}.

intermolecular hydrogen bonding in the H-bonded cluster $\mathbf{C_2}$ explains the more $q(O_{P=O})$ for the uncoordinated ligand $\mathbf{L_2}'$, compared to the free ligand $\mathbf{L_2}$. Similarly, along with increase in negative charge on the oxygen atom, hybridization of $LP(O_{P=O})$, $sp^{0.56}$, takes the more p character in $\mathbf{L_2}'$ *versus* $sp^{0.52}$ in $\mathbf{L_2}$. The electronic charge is transferred from the neighbors to the O atom involved in hydrogen bonding due to the polarization effect.

This electronic redistribution occurs even more when the ligand is coordinated to $SnPh_3Cl$, as the polarization effect arises from the electrostatic field of the Sn(IV) atom. Natural electronic configuration (NEC) of the $O_{P=O}$ atom is [core] $2s^{1.80}$ $2p^{5.25}$ in the free ligands that almost changes to [core] $2s^{1.76}$ $2p^{5.36}$ $3p^{0.01}$ by coordinating to the tin in $\mathbf{C_1}$. In the same way, electronic population in 2p orbital of the nitrogen increases from the free ligand $\mathbf{L_2}$ to the complex $\mathbf{C_2}$. The hybridization of the lone pair of the mentioned atoms, as expected, is affected upon complexation (Table 4). Furthermore, the atomic charges of donor sites become more negative when the ligand is coordinated. It is worth noting that the negative charge difference ($\Delta\delta^- = \delta^-(\text{donor atom})_{\text{complex}} - \delta^-(\text{donor atom})_{\text{free ligand}}$) is approximately equal for both the donors (0.067e for $O_{P=O}$ and 0.069e for N_{py}). The more value of $\Delta\delta^-$ (0.087e) is obtained for N_{py} using $\delta^-(N_{py})_{\text{free ligand}}$ of $\mathbf{L_2}'$ instead of $\mathbf{L_2}$. Other electronic differences between the ligands and the corresponding adducts can be viewed as a result of the intermolecular hydrogen bonds.

Structural preference of the complexes with the difunctional ligands

As mentioned in the previous part, the electronic properties of the ligands have not been significantly affected by the difference in the structures. This key result indicates that any differences between the $\mathbf{C_1}$ and $\mathbf{C_2}$ structures are not related to the electronic features of the ligands. In return, from the structural point of view, position of nitrogen in the pyridine ring on the one hand and the tendency of $SnPh_3Cl$ to produce a trigonal-bipyramidal stereochemistry on the other is of prime importance for the association. In the case of $\mathbf{C_1}$, coordination of the phosphoryl donor instead of *N*-pyridine which can be explained by steric hindrance, regardless of electronic priority (see section X-ray crystallography investigation).

Interestingly, the low preference of $\mathbf{L_2}$ for bidentate binding, despite the lack of steric demands, may be attributed to competition between two types of possible interactions for the P(O)NH functional group. It seems that the intermolecular $P=O\cdots HN_{amidic}$ interactions would be preferable to tin–oxygen coordination for the association in $\mathbf{L_2}$. To verify the assumption made above, we have carried out a comparative study on the real complex $\mathbf{C_2}$ and a model binuclear complex in which the bidentate ligand $\mathbf{L_2}$ adopts the bridging mode of coordination. As given in Table 5, the sum of two $P=O\cdots HN_{amidic}$ hydrogen-binding energies (13.28 kcal mol^{-1}) in $\mathbf{C_2}$ is larger than the energy gain from Sn–O interaction in the model (8.78 kcal mol^{-1}). This shows

that the monodentate binding mode of $\mathbf{L_2}$ is preferred, although the difference of ΔE with the bridging mode is small (4.50 kcal mol^{-1}). It should be stressed here that the highest occupied molecular orbital, HOMO, of the ligand $\mathbf{L_1}$ is localized on the *N*-pyridine atom, while the HOMO of $\mathbf{L_2}$ is located on the oxygen. Both of the mentioned atoms are involved in hydrogen bonding in the related complexes. It suggests that the coordinating modes adopted in both complexes are not only the result of stereo-electronic features of the donor sites but also of the influence of H-bonding interactions in the ligands.

Comparison between the coordination ability of the P=O and N_{py} functional groups

The NBO analysis of both ligands $\mathbf{L_1}$ and $\mathbf{L_2}$ shows that the hybridization of LP(N_{Py}) possesses a remarkable more p character in comparison with LP($O_{P=O}$). Furthermore, the natural electronic configuration of $O_{P=O}$ includes more electronic population in the electronegative 2s orbital ($2s^{1.8}$) compared to the case of N_{py} ($2s^{1.36}$). The obtained results reveal a higher electron availability and thus the higher basic potential of the nitrogen atom than the phosphoryl oxygen atom. In contrast, the negative charge on $O_{P=O}$ atom is approximately two times higher than that of N_{Py}, and makes the phosphoryl oxygen more suitable for the electrostatic interaction with the positive charged tin(IV) atom (about +2.1e). Finally, the influential electronic factor which determines the winner site depends on the type of substituents on the P atom.[10] In other words, the donor character of the P=O group depends on the electron donation ability of substituents, bounded to the phosphorus, and the magnitude of $q(O_{P=O})$. In the following, we will show that the former is more effective in the title ligands including two phenyl groups on the P atom.

Here the size of stabilizing energies E^2 for the electronic delocalization LP(donor) to LP*(Sn) can be used to characterize the strength of the donor–acceptor coordination interactions. Comparing the stabilizing energy of coordination bond in $\mathbf{C_1}$ (22.2. and 26.28 kcal mol^{-1}) and $\mathbf{C_2}$ (34.64 kcal mol^{-1}), it is found that the Sn–N_{py} is slightly stronger than the Sn–$O_{P=O}$ bond. This is also evident from Sn–Cl bond lengths in the model complex (Table 3). The longer distance belonging to the chlorine atom in *trans* position to N_{py} owing to the greater *trans* influence. Furthermore, the expected trend obtained for the stabilizing energies in the binuclear compound, although the difference is not very significant (Table 5). The higher electron donating capacity of N_{py} compared to $O_{P=O}$ is confirmed by the experimental results.

Hydrogen bonding

While the donor–acceptor distances of H-bonds in the hydrogen-optimized clusters are the same experimental values, the other optimized parameters differ from the X-ray values (Table 2). The DFT calculations yield the shorter DH···A distances compared to the solid state structures.

The NBO analysis reveals an electronic delocalization LP(A) → σ*(N–H) (A is N_{py} in $\mathbf{C_1}$ and $O_{P=O}$ in $\mathbf{C_2}$) among the subunits of the clusters. Such an electronic density transfer explains the lengthening of the N–H distances in the H-bonded clusters with respect to the fully optimized ligands. Table 5 shows that the stabilizing energy increases from the LP(N_{py}) → σ*(N–H) delocalization (5.02 and 13.66 kcal mol^{-1}) to LP($O_{P=O}$) → σ*(N–H) (10.80 and 10.24 kcal mol^{-1}), in line with a decrease in the donor–acceptor distance. Coincident with this, the values of 8.23 and 5.05 kcal mol^{-1} for binding energies were calculated for the $O_{P=O}$···H–N hydrogen bonds, while the ΔE value of 4.88 kcal mol^{-1} is related to the sum of two N_{py}···H–N interactions in the cluster $\mathbf{C_1}$.

The substantial contribution of the hydrogen bonds around 5–8 kcal mol^{-1} towards the stability of the resulting complexes makes these an essential factor for the interesting coordination behavior of the ligands. The influence of H-bonding on ligation manner of multifunctional compounds has also been realized previously.[3,30]

Experimental

Synthesis of ligands

The ligands were synthesized by the reaction of *n*-aminopyridine ($n = 2$ and 4 respectively) with $(C_6H_5)_2P(O)Cl$ in 2 : 1 molar ratio. The amine was added dropwise to a CH_3CN solution (20 ml) of $(C_6H_5)_2P(O)Cl$ at 0 °C. After 24 h, the solvent was evaporated and the residue was washed with distilled water and dried. Physical and spectroscopic data of them are presented below:

***N*-(2-pyridinyl)diphenylphosphinic amide ($\mathbf{L_1}$)..**[8] Yield: 85%. m.p. 176 °C. Anal. calc. for $C_{17}H_{15}N_2OP$: C 69.38, H 5.13, N 9.52; found: C, 69.16; H, 5.21; N, 9.26.^{31}P NMR (121.49 MHz, $CDCl_3$): δ (ppm) = 18.8. ^{1}HNMR (300.13 MHz, $CDCl_3$): δ (ppm) = 6.77 (ddd, $^3J_{HH}$ = 7.3 Hz, $^3J_{HH}$ = 5.0 Hz, $^6J_{PH}$ = 0.8 Hz, 1H-py), 6.99 (d, $^3J_{HH}$ = 8.3 Hz, 1H-py), 7.39–7.55 (m, 6H-Ph, 1H-py), 7.90 (dd, $^3J_{HH}$ = 6.8 Hz, $^3J_{PH}$ = 12.6 Hz, 4H; *o*-Ph), 7.98 (d, $^3J_{HH}$ = 5.0 Hz, 1H-py). IR (KBr, cm^{-1}): ν = 3117 (m, NH), 1591 (s, py ring), 1185 (*vs.*, P=O).

***N*-(4-pyridinyl)diphenylphosphinic amide ($\mathbf{L_2}$).** Yield: 72%. m.p. 193 °C. Anal. calc. for $C_{17}H_{15}N_2OP$: C 69.38, H 5.13, N 9.52; found: C, 69.14; H, 5.19; N, 9.36%. ^{31}P NMR (121.49 MHz, $CDCl_3$): δ (ppm) = 19.5. ^{1}H NMR (300.13 MHz, $CDCl_3$): δ (ppm) = 6.85 (d, $^3J_{HH}$ = 6.2 Hz, 2H-py), 7.44 (td, $^3J_{HH}$ = 6.1 Hz, $^4J_{PH}$ = 3.4 Hz, 4H; *m*-Ph), 7.53 (t, $^3J_{HH}$ = 7.2 Hz, 2H; *p*-Ph), 7.81 (dd, $^3J_{HH}$ = 7.0 Hz, $^3J_{PH}$ = 12. 7 Hz, 4H; *o*-Ph), 8.14 (d, $^3J_{HH}$ = 6.1 Hz, 2H-py). IR (KBr, cm^{-1}): ν = 3203 (s, NH), 1595 (s, py ring), 1182 (*vs.*, P=O).

Synthesis of complexes

***N*-(2-pyridinyl)diphenylephosphinic amide-κ-*O* chlorotriphenyltin(IV) ($\mathbf{C_1}$).** 0.1 mmol triphenyltinchloride (0.04 g) was added to a solution of 0.1 mmol ligand 1 (0.03 g) in 10 ml chloroform and the mixture stirred for some hours. The single crystals suitable for X-ray analysis were isolated by slow evaporation of a 1 : 1 solution chloroform–heptan at room temperature. Yield: 85%. m.p: 150 °C. Anal. calc. for $C_{35}H_{30}ClN_2OPSn$ (679.77): C, 61.84; H, 4.44; N, 4.12. Found: C, 61.79; H, 4.65; N, 4.14%. ^{31}P NMR (121.49 MHz, $CDCl_3$): δ (ppm) = 18.8. ^{1}H NMR

(300.13 MHz, $CDCl_3$): δ (ppm) = 6.77 (dd, $^3J_{HH}$ = 7.3 Hz, $^3J_{HH}$ = 5.1 Hz, 1H-py), 6.94 (d, $^3J_{HH}$ = 8.3 Hz, 1H-py), 7.36–7.70 (m, 22H; H-Ph, py), 7.87 (dd, $^3J_{HH}$ = 8.1 Hz, $^3J_{PH}$ = 12.6 Hz, 4H; *o*-Ph), 7.98 (d, $^3J_{HH}$ = 4.5 Hz, 1H-py). ^{119}Sn NMR (111.86 MHz, $CDCl_3$): δ (ppm) = −50. IR (KBr, cm^{-1}): ν = 3442 (s, NH), 1591 (s, py ring), 1161 (*vs*, P═O).

***N*-(4-pyridinyl)diphenylephosphinic amide-κ-*N* chlorotriphenyltin(IV). *N*-(4-pyridinyl)diphenylphosphinic amide (C_2).** 0.2 mmol triphenyltinchloride (0.04 g) was added to a solution of 0.1 mmol ligand 3 (0.03 g) in 10 ml chloroform and the mixture stirred for some hours. The suitable crystals for X-ray analysis were obtained by slow evaporation of a 1 : 1 solution chloroform–heptane at room temperature. Yield: 55%. m.p: 110 °C. Anal. calc. for $C_{52}H_{45}ClN_4O_2P_2Sn$ (974.02): C, 64.12; H, 4.65; N, 5.75. Found: C, 64.16; H, 4.26; N, 5.83%. ^{31}P NMR (121.49 MHz, $CDCl_3$): δ (ppm) = 19.6. ^{1}H NMR (300.13 MHz, $CDCl_3$): δ (ppm) = 6.86 (d, $^3J_{HH}$ = 6.2 Hz, 4H-py), 7.15 (br, NH), 7.32–7.70 (m, 27H; H-Ph), 7.82 (dd, $^3J_{HH}$ = 6.9 Hz, $^3J_{PH}$ = 12.7 Hz, 8H; *o*-Ph), 8.08 (d, $^3J_{HH}$ = 5.7 Hz, 4H-py). ^{119}Sn NMR (111.86 MHz, $CDCl_3$): δ (ppm) = −74. IR (KBr, cm^{-1}): ν = 3440 (s, NH), 1614 (m, py ring), 1187 (m, P═O).

Instrumentation

^{1}H, ^{31}P and ^{119}Sn NMR spectra were recorded on a Bruker-Avance DRS 500 spectrometer at 300.13, 121.50 and 111.86 MHz, respectively. ^{1}H, ^{31}P and ^{119}Sn chemical shifts were measured relative to $Si(CH_3)_4$, 85% H_3PO_4 and $Sn(CH_3)_2$ as external standard respectively. Infrared (IR) spectra were recorded on KBr disk using a Shimadzu model IR-60 spectrometer. Elemental analysis was performed using a Heraeus CHN-O-RAPID apparatus. Melting points were obtained with an electrothermal instrument.

Crystal structure determination

Bragg-intensities of the $\mathbf{C_1}$ and $\mathbf{C_2}$ were collected (T = 292 K) on a Stoe IPDS II with graphite-monochromatized MoKα (λ = 0.71073 Å) radiation. Cell refinement and integration by X-AREA (1.62),[36] data reduction and a numerical absorption correction by XRED32 (1.31).[37] $\mathbf{C_1}$ was solved with direct methods (SHELXS-97)[38] and $\mathbf{C_2}$ with DIRDIF-2008.[39] Refinement on $|F|^2$ with the program SHELXL-97.[38] All non-H atoms in $\mathbf{C_1}$ and $\mathbf{C_2}$ were refined anisotropically and the aromatic H were made to ride on their carrier atoms, except the amine-H which were optimized isotropically after having been located in a difference map. In $\mathbf{C_1}$ most of the carbons appeared as prolate ellipsoids; the worst rings C17 → C21 and C72 → C77 were split into two, their s.o.f. adding up to one. Nevertheless, SAME, ISOR and FLAT restraints had to be imposed in order to hinder them from diverging. SAME restraints also had to be used for obtaining reasonable Sn–C distances. The crystallographic and refinement data are summarized in Table S1† for both complexes.

Computational details

Density functional theory (DFT) calculations were carried out using the Gaussian 03 program-package.[40] In the case of $\mathbf{C_1}$ and $\mathbf{C_2}$, the X-ray structures of complexes were used as starting points for the geometrical calculation. For the structure $\mathbf{C_1}$ two hydrogen-bonded conformers were used in the calculations, while the structure $\mathbf{C_2}$ was modelled as a cluster in which the target complex is surrounded by two neighbouring uncoordinated ligands. Although normalized hydrogen positions from Mo-data are also quite reliable, we preferred to optimize the hydrogen atoms, and kept all other atoms invariant in the optimization process. We denote these structures as hydrogen-optimized systems. Moreover, full geometrical optimizations of the ligands and a binuclear model (wherein the ligand $\mathbf{L_2}$ is bridged between two $SnPh_3Cl$ moieties) were computed. The calculations were performed at the B3LYP/6-311G* level of theory[41] for all atoms except the tin(IV) which were described by the LanL2DZ basis set[42] without any symmetry restrictions. The electronic features of the optimized structures were studied by natural bound orbital[43](NBO) analysis at the B3LYP method and the LanL2DZ and 6-311+G* basis sets. Besides, some surprising binding energies were calculated for the binuclear model and the real hydrogen-bonded clusters based on the energy difference between the total energy of the systems and their fragments, as represented in the equation $\Delta E = E_{total} - (E_{frag1} + E_{frag2})$. Fragments 1 and 2 are two subunits which are connected by the corresponding bond. The interaction energies were corrected for basis set superposition error (BSSE) based on the counterpoise correction method of Boys and Bernardi.[44]

Conclusion

We have prepared and characterized two organotin(IV) adducts with phosphoramidate derivatives based on aminopyridine as heterodifunctional ligands. The crystal structures of the complexes reveal Sn(IV) to be five-coordinated and both ligands to function in an ambidentate mode. The ligand $\mathbf{L_1}$ coordinates *via* a phosphoryl group in the structure $\mathbf{C_1}$, while the other one acts as an N-donor in the crystal $\mathbf{C_2}$. The calculations of the complexes in the gas phase, with respect to the solid-state structures and the chemical behavior in solution, are compatible with each other; they show that Sn(IV) interacts more strongly with the N-atom in pyridine than the with the P═O functional group. In the case of $\mathbf{C_1}$, coordination of the phosphoryl donor instead of N-pyridine can be explained by steric hindrance, regardless of the electronic priorities. In contrast, the low preference of $\mathbf{L_2}$ for bidentate binding, despite the lack of steric demands, can be attributed to a competition between two types of possible interactions for the P(O)NH functional group. Indeed, theoretical calculations indicate the intermolecular P═O···HN_{amidic} interactions would be preferable to tin–oxygen coordination for the association in $\mathbf{C_2}$. The substantial contribution of the hydrogen bonds around 5–8 kcal mol^{-1} towards the stability of the resulting complexes makes these an essential factor for the interesting coordination behavior of both ligands.

Acknowledgements

Financial support of this work by Tarbiat Modares University is gratefully acknowledged.

Notes and references

1 V. V. Grushin, *Chem. Rev.*, 2004, **104**, 1629.
2 S. M. Aucott, A. M. Z. Slawin and J. D. Woollins, *Dalton Trans.*, 2000, 2559.
3 A. M. Z. Slawin, J. Wheatley, M. V. Wheatley and J. D. Woollins, *Polyhedron*, 2003, **22**, 1397.
4 D. A. Padron and K. K. Klausmeyer, *Inorg. Chim. Acta*, 2013, **405**, 511.
5 D. A. Padron and K. K. Klausmeyer, *Inorg. Chim. Acta*, 2013, **405**, 511.
6 S. Pailloux, C. E. Shirima, A. D. Ray, E. N. Duesler, K. A. Smith, R. T. Paine, J. R. Klaehn, M. E. McIlwainb and B. P. Hay, *Dalton Trans.*, 2009, 7486.
7 F. D. Sokolov, N. G. Zabirov, L. N. Yamalieva, V. G. Shtyrlin, R. R. Garipov, V. V. Brusko, A. Y. Verat, S. V. Baranov, P. Mlynarz, T. Glowiak and H. Kozlowski, *Inorg. Chim. Acta*, 2006, **359**, 2087.
8 W. Lackner-Warton, S. Tanaka, C. M. Standfest-Hauser, Ö. Öztopcu, J. Hsieh, K. Mereiter and K. Kirchner, *Polyhedron*, 2010, **29**, 3097.
9 A. D. Garnovskii, D. A. Garnovskii, I. S. Vasil'chenko, A. S. Burlov, A. P. Sadimenko and I. D. Sadekov, *Russ. Chem. Rev.*, 1997, **66**, 389.
10 K. Gholivand, N. Oroujzadeh and F. Afshar, *J. Organomet. Chem.*, 2010, **695**, 1383.
11 K. Gholivand, S. Farshadian and Z. Hosseini, *J. Organomet. Chem.*, 2012, **696**, 4298.
12 K. Gholivand and S. Farshadian, *Inorg. Chim. Acta*, 2011, **368**, 111.
13 K. Gholivand, N. Oroujzadeh and M. Rajabi, *J. Iran. Chem. Soc.*, 2012, **9**, 865.
14 K. Gholivand, H. R. Mahzouni, M. Pourayoubi and S. Amiri, *Inorg. Chim. Acta*, 2010, **363**, 2318.
15 K. Gholivand, M. Rajabi, F. Molaei, H. R. Mahzouni and S. Farshadian, *J. Coord. Chem.*, 2013, **66**, 4199.
16 S. E. Denmark and J. J. Fu, *J. Am. Chem. Soc.*, 2003, **125**, 2208.
17 S. E. Denmark, T. Wynn and G. L. Beutner, *J. Am. Chem. Soc.*, 2002, **124**, 13405.
18 S. K. Hadjikakou and N. Hadjiliadis, *Coord. Chem. Rev.*, 2009, **253**, 235.
19 X. Shang, X. Meng, E. C. B. A. Alegria, Q. Li, M. F. C. Guedes da Silva, M. L. Kuznetsov and A. J. L. Pombeiro, *Inorg. Chem.*, 2011, **50**, 8158.
20 E. López-Torres, F. Zani and M. A. Mendiola, *J. Inorg. Biochem.*, 2011, **105**, 600.
21 T. Gianferrara, I. Bratsos and E. Alessio, *Dalton Trans.*, 2009, **37**, 7588.
22 D. R. Smyth, C. P. D. Stapleton and E. R. T. Tiekink, *Organometallics*, 2003, **22**, 4599.
23 R. Zhang, G. Tian and C. Ma, *J. Organomet. Chem.*, 2005, **690**, 4049.
24 C. L. Ma, Y. F. Han, R. F. Zhang and D. Q. Wang, *Dalton Trans.*, 2004, 1832.
25 R. Murugavel, R. Pothiraja, S. Shanmugan, N. Singh and R. J. Butcher, *J. Organomet. Chem.*, 2007, **692**, 1920.
26 K. E. Gubina, V. A. Ovchynnikov, J. Swiatek-Kozlowska, V. M. Amirkhanov, T. Yu. Sliva and K. V. Domasevitch, *Polyhedron*, 2002, **21**, 963.
27 Wrackmeyer, in: *Tin Chemistry: Fundamentals, Frontiers, and Applications*, ed. A. G. Davies, M. Gielen, K. H. Pannell, E. R. T. Tiekink, Wiley, Chichester, UK, 2008, ch. 2, pp. 17–53.
28 J. Lorberth, S. Wocadlo, W. Massa, E. V. Grigoriev, N. S. Yashina, V. S. Petrosyan and P. Finocchiaro, *J. Organomet. Chem.*, 1996, **510**, 287; M. Wagner, M. Henn, C. Dietz, M. Schürmann, M. H. Prosenc and K. Jurkschat, *Organometallics*, 2013, **32**, 2406; B. Z. Momeni, S. Shahbazi and H. R. Khavasi, *Polyhedron*, 2010, **29**, 1393.
29 J. Holecek, M. Nadvornik, K. Handlir and A. Lycka, *J. Organomet. Chem.*, 1986, **315**, 299.
30 A. R. Salimi, M. Mirzaei, M. Chahkandi, A. Azadmeher, H. Eshtiagh-Hosseini, H. R. Khavasi and M. M. Amini, *J. Mol. Struct.*, 2009, **937**, 44.
31 R. Zhang, M. Yang and C. Ma, *J. Organomet. Chem.*, 2008, **693**, 2551.
32 A. Bondi, *J. Phys. Chem.*, 1964, **68**, 441.
33 A. R. Narga, M. Schuermann and C. Silvestru, *J. Organomet. Chem.*, 2001, **623**, 161.
34 S. Chandrasekar, B. S. Krishnamoorthy, V. S. Sridevi and K. Panchanatheswaran, *J. Coord. Chem.*, 2005, **58**, 295.
35 M. Nishio, *CrystEngComm*, 2004, **6**, 130.
36 *X-AREA, Version 1.62*, Stoe and Cie, Darmstadt, Germany, 2011.
37 *X-RED32, Version 1.31*, Stoe and Cie GmbH, Darmstadt, Germany, 2005.
38 G. M. Sheldrick, *Acta Crystallogr.*, 2008, **A64**, 112.
39 P. T. Beurskens, G. Beurskens, R. De Gelder, J. M. M. Smits, S. García-Granda and R. O. Gould, DIRDIF, *Crystallography Laboratory*, Radboud University Nijmegen, The Netherlands, 2007.
40 M. J. Frisch, *et al.*, *Gaussian 03, Revision D.01*, Gaussian, Inc., Wallingford, CT, 2004.
41 C. Lee, W. Yang and R. G. Parr, *Phys. Rev. B: Condens. Matter Mater. Phys.*, 1988, **37**, 785.
42 P. J. Hay and W. R. Wadt, *J. Chem. Phys.*, 1985, **82**, 299.
43 P. Foster and F. Weinhold, *J. Am. Chem. Soc.*, 1980, **102**, 7211.
44 S. F. Boys and F. Bernardi, *Mol. Phys.*, 1970, **19**, 553.